AUTO-COMBUSTION SYNTHESIZED Ni (Mg, Cu, Co) Fe_2O_4 FOR IMPEDANCE AND GAS SENSING STUDIES

Rajesha Shetty G[1], Shilpa S[2], Raviraja S[3], L. N Shubha[4], S. Abdul Khader[5]*, Asiya Parveez[5]
[1]Department of Physics, Govt. First Grade College for Women, Balmatta, Mangalore-575001, Karnataka, India.
[2]Department of Physics, Govt. First Grade College, Kadugudi, Bengaluru-560067, Karnataka, India.
[3]Department of Physics, Govt. First Grade College, Thenkandiyur, Udupi- 576106, Karnataka, India.
[4]Department of Physics, St. Francis College for Women (Autonomous), Begumpet, Hyderabad-500016.
[5]Department of Physics, Govt. Science College, Chitradurga-577501, Karnataka, India.
Corresponding Author: S. Abdul Khader, khadersku@gmail.com

Abstract:

This article presents the impedance and magnetic studies of divalent metal ions doped nickel ferrite. Divalent metal ions such as Mg+2, Cu+2 and Co+2 were substituted in pure Nickel ferrite (NiFe2O4) with the basic composition Ni0.5M0.5Fe2O4 (here, M= Mg+2, Cu+2 and Co+2), which were synthesized by auto-combustion method using, nitrate-citrate method. Synthesized samples were sintered at 9500C and investigated for various properties. Phase of the synthesized samples were probed by X-ray diffraction (XRD) studies. Peaks observed in the XRD spectrum confirms the single phase spinel cubic structure for the divalent metal ions substituted NiFe2O4. Using FESEM, surface morphology of the samples has been investigated. Composition and frequency dependent dielectric and impedance properties were studied using HIOKI make LCR meter model 3520-50 from 20 Hz to 5 MHz. For the proposed nano-powder samples gas sensing measurements were done at RT to sense NO2.

Keywords: Impedance; Phase; Nano-powders; Sensing; Precursors.
DOI Number: 10.48047/nq.2021.19.2.NQ21043 **NeuroQuantology 2021; 19(2): 253-260**

Introduction

Mostly used ferrites in the ferrite family are spinel ferrites. Nano structured soft spinel ferrites have attracted great interest due to their excellent physio-chemical properties such as , low toxicity and their magnetism as well as, because of their highly tunable properties, like its dielectric, magnetic properties, which can be easily modified just adopting various preparation techniques and various factors such as the type of organic fuel used for the synthesis, P_H of the redox solution, composition of the metal ions, crystal structure, types of additives and sintering temperature etc [1-3]. These nano-structured magnetic oxides are currently considered among the widely successful magnetic nanoparticles (MNPs) that can be extensively used for various technological and in medical applications such as electrochemical sensor applications, in storage medium, contrast enhancement in magnetic resonance imaging, suspension systems using magnetic fluids, targeted drug delivery and in many more technological devices and applications. [4-5].

Spinel magnetic oxide materials, mainly consists of Fe_2O_3 and have spinel (MFe_2O_4) cubic structure, here M is a divalent metal ion such as Co^{+2}, Zn^{+2}, Mg^{+2}, Ni^{+2}, Cd^{+2}, Cu^{+2} or a combination of these ions. These samples,

which are ferri-magnetic in nature exhibit magnetic hysteresis (M-H curve) and at the same time exhibit spontaneous magnetization. Various properties of magnetic spinel is because of distribution of divalent and trivalent metal ions among the available voids such as tetrahedral (A) and octahedral (B) sites [5]. For any materials of interest, its properties are highly dependent on preparation technique adopted, type of synthesis environment such as in inert or in open air atmosphere, type of organic fuel used, sintering time and temperature, etc.

In case of inverse spinel structure half of the trivalent metal ions occupy tetrahedral (A-sites) and half in octahedral (B-sites), the remaining cations being randomly distributed among the B-sites. Inverse spinel ferrites are represented by the formula $(Me^{+3})_A [M^{+2}Me^{+3}]_B O_4$. Nickel ferrite belongs to inverse spinel with Ni^{+2} at octahedral (B-site) and Fe^{+3} ions distributed equally in both, tetrahedral (A-site) and octahedral sites (B-site). Nickel ferrites are used in numerous electronic device applications because of their high permeability, high electrical resistivity, mechanical hardness, and chemical stability [6-10].

Samples of divalent metal ions substituted nickel ferrite are the technologically important materials which are used in functional devices such as in field sensors, heterogeneous catalysis, and in various sensors [11].

In our present study, samples of divalent metal ions substituted nickel ferrite with the basic composition $Ni_{0.5}M_{0.5}Fe_2O_4$ (here M= Mg^{+2}, Cu^{+2} and Co^{+2}) were prepared using nitrate-citrate auto-combustion method. This method is a self-propagating thermally-induced reaction of a gel, obtained from aqueous solutions containing metallic nitrates which acts as oxidizer and an organic fuel. Stoichiometric proportions between fuel and metallic nitrates are calculated according to the valencies of the reacting elements so as to provide the relation of oxidizer/fuel equal to one [12]. Here, metallic nitrates are preferred as starting materials which are also known as precursors, because of their water-soluble nature, have low ignition temperatures and are easy to prepare.

Materials and methods

Nano-powders of divalent metal ions substituted $NiFe_2O_4$ ferrite samples of $Ni_{0.5}M_{0.5}Fe_2O_4$ a, here M = Mg^{+2}, Cu^{+2} and Co^{+2} were prepared using auto-combustion method. Precursors for starting the materials synthesis are Nickel Nitrate ($Ni(NO_3)_2.6H_2O$), Ferric Nitrate ($Fe(NO_3)_2.9H_2O$), Magnesium Nitrate ($Mg(NO_3)_2.6H_2O$), Copper Nitrate ($Cu(NO_3)_2.3H_2O$, Cobalt Nitrate ($Co(NO_3)_2.6H_2O$) and Citric acid ($C_6H_8O_7.H_2O$), all chemicals are of AR Grade with purity more than 99%. Aqueous solutions of metallic nitrates and Citric acid, which is here taken as organic fuel needed for auto-combustion reaction and are taken as per the stoichiometry. Equi-molar citric acid was added into the aqueous solution of metallic nitrates. Aqueous solution containing redox mixture was taken in a silica crucible and is allowed in to a muffle furnace, which was already pre-heated to a temperature of 550^0C. Redox mixture finally yields porous and fluffy voluminous ferrite powder. Obtained fluffy material was ground to get ferrite powders. As-burnt ash was sintered at 950^0C for 4 hours to get better crystallization and homogeneous cation distribution in the proposed spinel and finally ground to get proposed ferrite nano-powders. Phase confirmation of the proposed samples were investigated using X-ray diffraction (XRD) studies using Bruker AXS D8 Advance X-ray diffractometer (using Cu-K_α radiation, λ=1.5406 Å), a working voltage of 40kV at 40mA of current. Diffraction data were collected in the 2θ range 10-80^0. Morphology of the sintered samples has been investigated using Field Emission Scanning Electron Microscope (JEOL Model 7610FPLUS). Parallel capacitance, C_p and dissipation factor, tanδ as a function of frequency in the range 20 Hz-5 MHz were measured using a precision LCR meter. Real and imaginary parts of Impedance (Z' and Z'') dielectric permittivity (ε') and (ε'') were computed using the formulae [13],

$$\varepsilon' = Ct/\varepsilon_0 A \quad (1)$$

$$\varepsilon'' = \varepsilon' \tan\delta \quad (2)$$

Where, t is the thickness and A, the area of the pellet.

The ac conductivity, σ_{ac} was determined from the dielectric loss factor using a relation

$$\sigma_{ac} = \omega \varepsilon_0 \varepsilon'' \quad (3)$$

Where, ε_0 is the vacuum permittivity and $\omega = 2\pi f$ with f being frequency.

Results and discussion

Phase and Surface Morphology

XRD diffractograms of the proposed samples of the system $Ni_{0.5}M_{0.5}Fe_2O_4$ (here M= Mg^{+2}, Cu^{+2}, Co^{+2}) are presented in Figure 1(a) and Fig 1(b). Presence of (220), (311), (400), (422), (511), (440) and (533) planes indexed for the cubic phase of spinel ferrites [For $Ni_{0.5}Mg_{0.5}Fe_2O_4$, JCPDS Card No: 52-0278 and JCPDS Card No: 77-0010 for $Ni_{0.5}Cu_{0.5}Fe_2O_4$ and for $Ni_{0.5}Co_{0.5}Fe_2O_4$, JCPDS Card No: 25-0283]. Synthesized nano-samples were labelled as NMg-2 ($Ni_{0.5}Mg_{0.5}Fe_2O_4$), NCu-2 ($Ni_{0.5}Cu_{0.5}Fe_2O_4$) and NCo-2 for $Ni_{0.5}Co_{0.5}Fe_2O_4$. Microstructures were studied by placing the samples under Scanning electron microscope. Micrographs of the sintered samples are depicted in Fig. 2 (a-c), shows the surface structure for the proposed samples. All the samples are having well dispersed, dense and well defined granular structure.

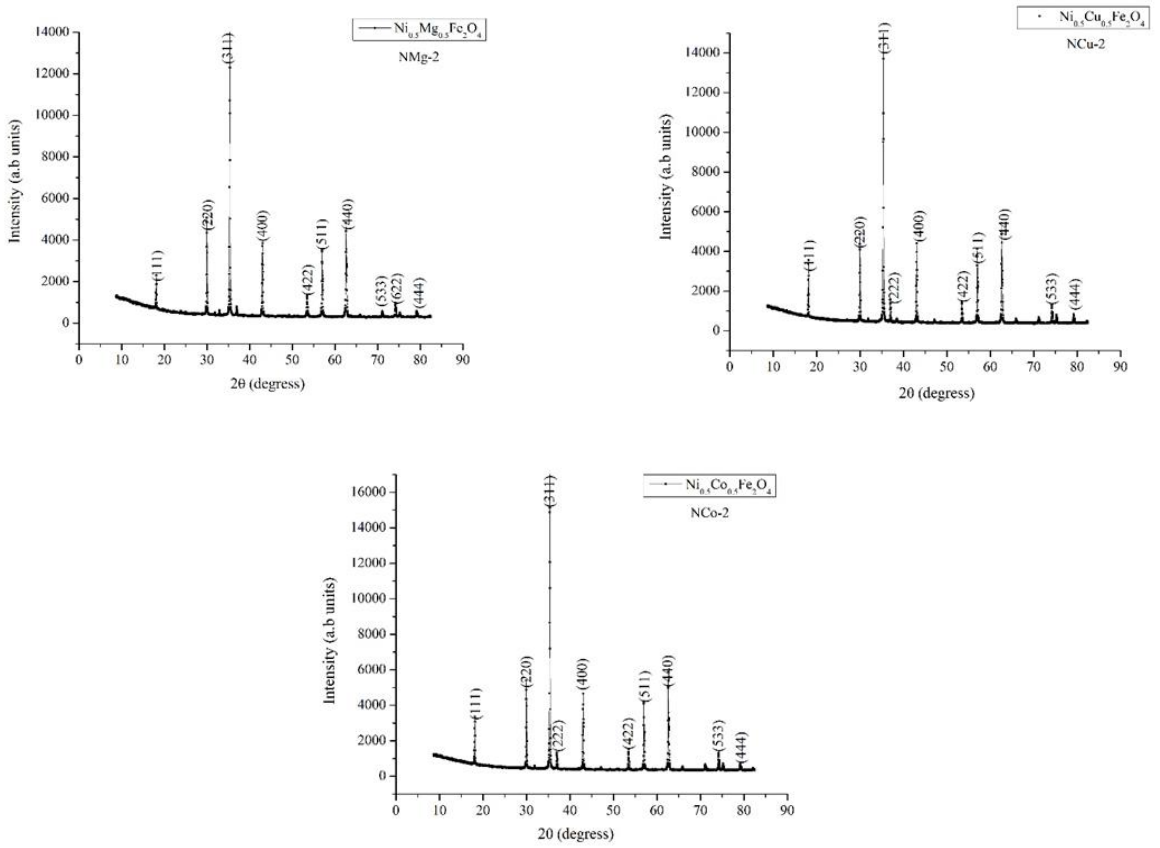

Fig. 1. XRD Spectrum of (a) $Ni_{0.5}Mg_{0.5}Fe_2O_4$, (b) $Ni_{0.5}Cu_{0.5}Fe_2O_4$ and (c) $Ni_{0.5}Co_{0.5}Fe_2O_4$

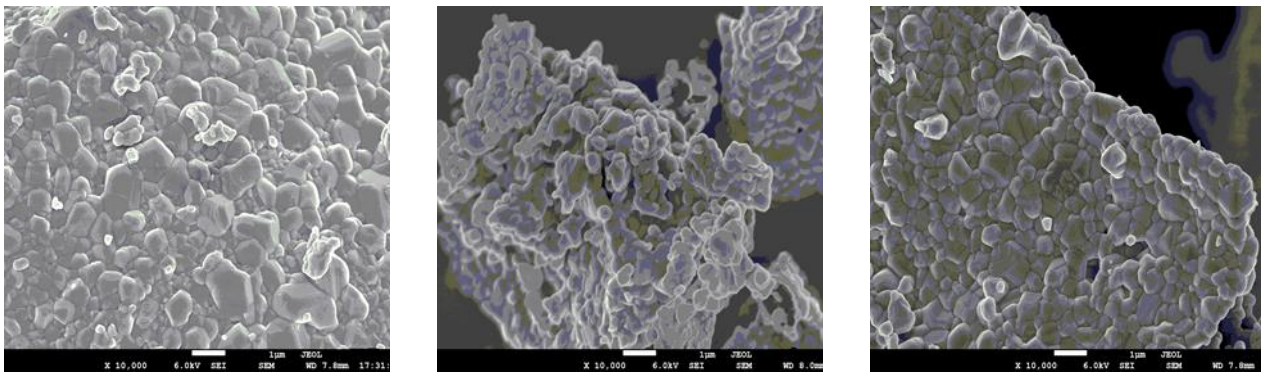

Fig. 2 Micrographs of (a) $Ni_{0.5}Mg_{0.5}Fe_2O_4$ (b) $Ni_{0.5}Cu_{0.5}Fe_2O_4$ (c) $Ni_{0.5}Co_{0.5}Fe_2O_4$

Dielectric and Impedance Studies

Impedance analysis was carried out at RT to study the RLC behavior of the proposed samples in the frequency range from 20 Hz to 5 MHz, these impedance measurements provides information about resistive (Z') and reactive (Z'') contributions in any ferromagnetic materials. In general, the total impedance acts as pure resistance at lower frequencies and pure capacitance at higher frequencies. Obtained impedance data is fitted or compared with an equivalent RLC circuit. In this equivalent RLC circuit, capacitance and inductance will be generally associated with space charge polarization regions. Data obtained from impedance studies is analyzed in terms of four complex formalisms namely Impedance (Z^*), electric modulus (M^*), permittivity (ε^*) and the admittance (Y^*) and these are related by,

$$M^* = J\omega C_0 Z^* \text{ and } Y^* = J\omega C_0 \varepsilon^* \quad (4)$$

Here, **ω** is the angular frequency, $\mathbf{C_0}$ is the vacuum capacitance of the measuring cell and electrodes without the actual sample. Curves for real and imaginary parts of impedance and electric modulus are shown in Figures from Fig 3(e) to 3 (j). Electric modulus is used to investigate the conduct of interfacial polarization in relation to the frequency of applied field. Bends in the middle of modulus curves, M' Vs M'' will give a detailed information of grain boundary or grain partition related contribution towards conduction mechanism.

Dielectric parameters such as permittivity, ε' and ac conductivity (σ_{ac}) with respect to variation in frequency at room temperature for the synthesized samples is shown in Fig.3. From the Fig.3 (a), it is clear that ε' decreases with increasing frequencies and remains almost independent at higher frequencies. Variation of dielectric constant with applied frequency is due to charge transport relaxation. Dielectric dispersion is common in ceramics like ferrites and is attributed to Maxwell and Wagner type of interfacial polarization [14-15], as the dielectric constant is a combined effect of dipolar, electronic, ionic and interfacial polarizations. Since ionic polarization decreases with frequency, at higher frequency cycle rates, the constituent electric dipoles are unable to follow the quick variations of the alternating applied electric field and hence, measured ε' also decreased with frequency. Larger values of permittivity are related with space charge polarization at grain boundary and heterogeneous dielectric structure.

By electron exchange between Fe^{+2} and Fe^{+3}, displacement of electrons takes place with the applied field and these electrons determine polarization. Polarization decreases with increase in frequency and for further increase, the electric exchange between Fe^{+2}/Fe^{+3} cannot follow the alternating field hence reaches the constant value [16-17].

Variation in the dielectric loss for all the proposed series of samples upto the frequency range of 5 MHz at room temperature is shown in Fig. 3(d). Values of loss tangent (tanδ) represent the attenuation in these proposed ceramics and polarization being unable to respond to applied external frequency. Similar nature of curves for both ε' and tanδ are almost similar and may be correlated to the domain wall motion with the applied field, the electron exchange between Fe^{+2} and Fe^{+3} ions can correlate with the dielectric properties exhibited by proposed samples.

In order to understand the type of charge carriers and type of polarons responsible for conduction, ac conductivity, σ_{ac} were estimated as per $\sigma_{ac} = \omega \varepsilon_0 \varepsilon''$, with ε_0 is the permittivity of free space and $\omega = 2\pi f$.

For the synthesized samples, variation of a.c conductivity, σ_{ac} with frequency, ln (ω), is shown in Fig.3 (c). Obtained plots are almost linear for the entire range of frequency except at lower frequencies. Linear variation of σ_{ac} with frequency confirms that, conduction in mixed spinel ferrite occurs by the hopping of charge carriers between the localized states which confirms the small polaron type of conduction [18]. Conduction mechanism in spinel ferrites can be explained based on the hopping of charge carriers between Fe^{+2} and Fe^{+3} ions on octahedral lattice sites. Increase in the frequency of the applied field accelerates the hopping of charge carriers thereby enhancing the overall conduction process, thereby increasing the conductivity. At higher frequencies, ac conductivity (σ_{ac}),

remains constant because the hopping frequency of the charge carriers no longer follows the external applied field variations and lags behind it. However, the decrease in conductivity values at lower frequencies can be correlated to conduction by mixed polarons.

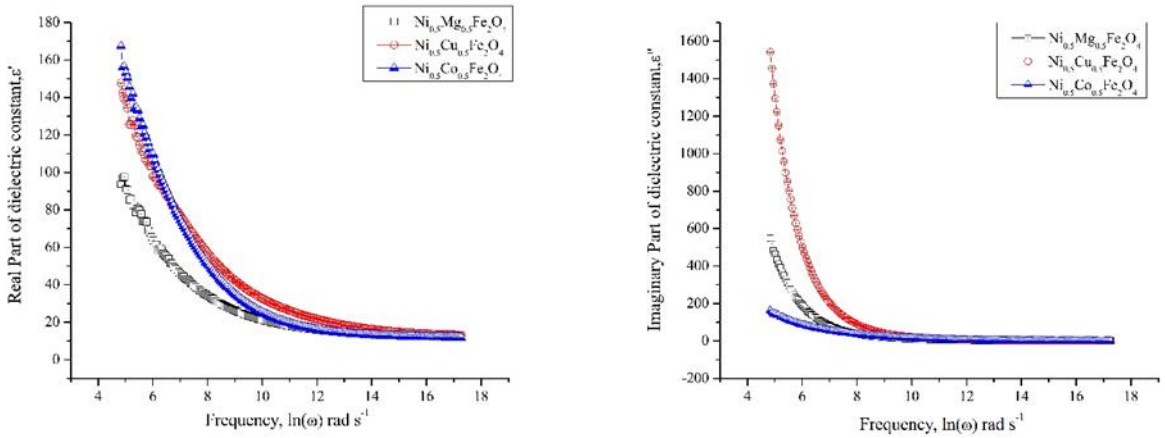

Fig. 3 Variation of (a). Real Part of Dielectric constant, ε' with ln(ω) and (b) Imaginary Part of Dielectric constant, ε" with ln(ω).

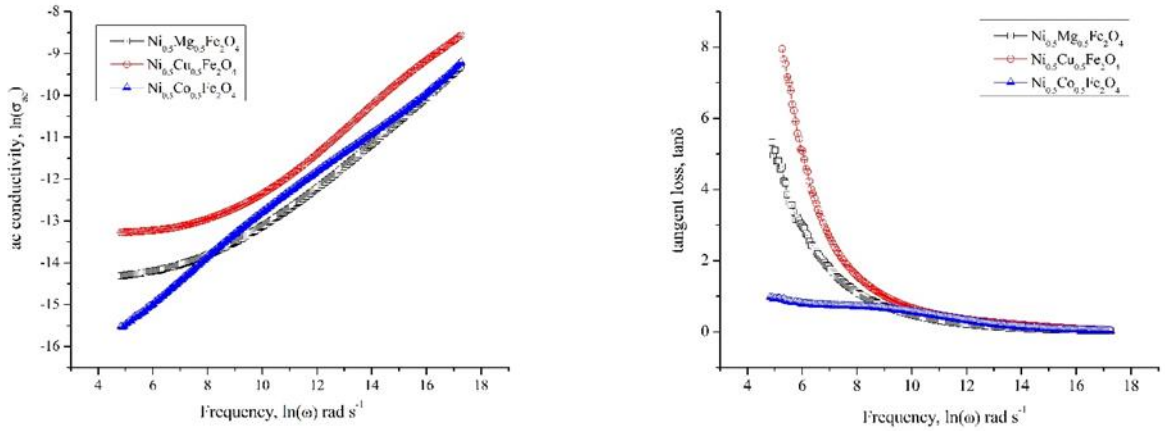

Fig. 3 Variation of (c) AC conductivity, ln (σ_{ac}) with ln(ω) and (d) Tangent loss factor tanδ with ln(ω).

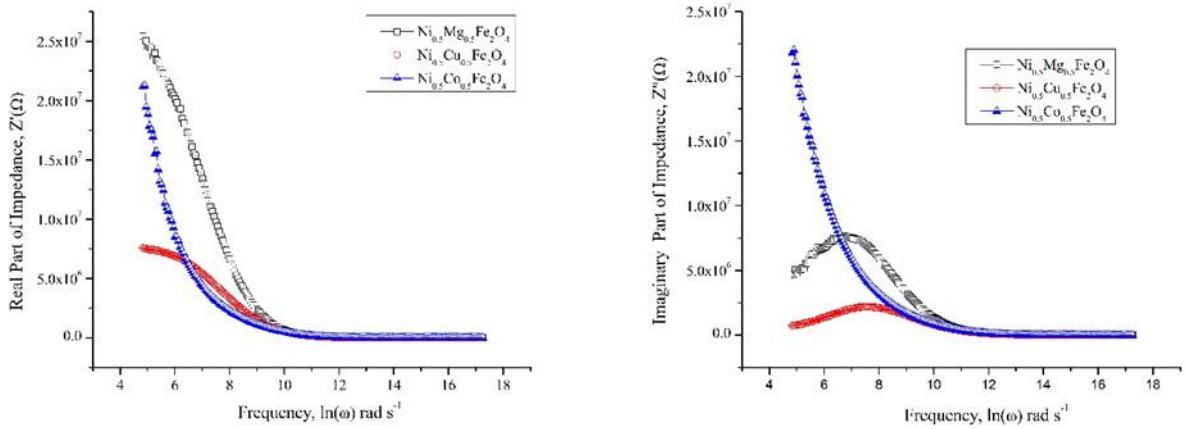

Fig. 3 Variation of Real and Imaginary Parts of (e) Z' and Z" with ln(ω) and (f) electric modulus M' and M" with ln(ω).

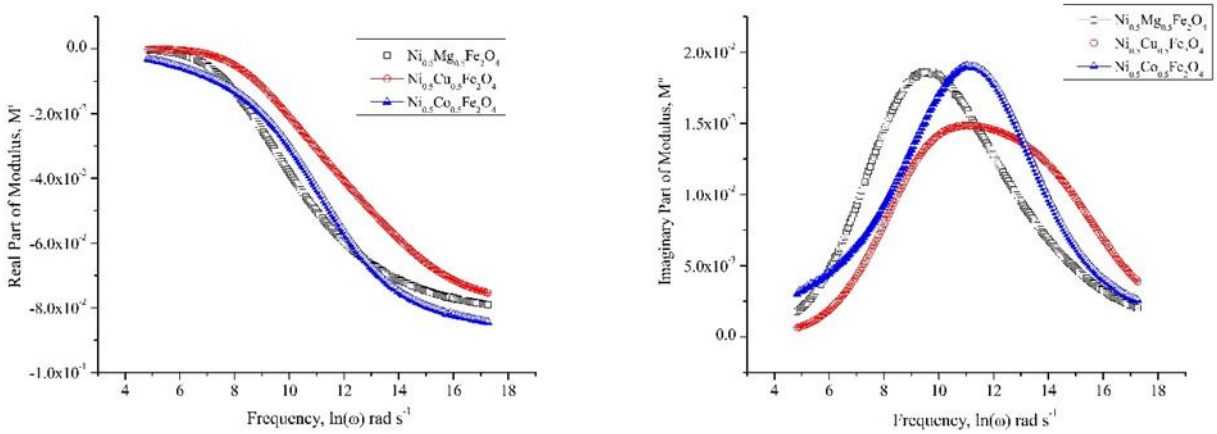

Fig. 3 Variation of Real and Imaginary Parts of electric modulus (g) M' with ln (ω) and (h) M" with ln(ω).

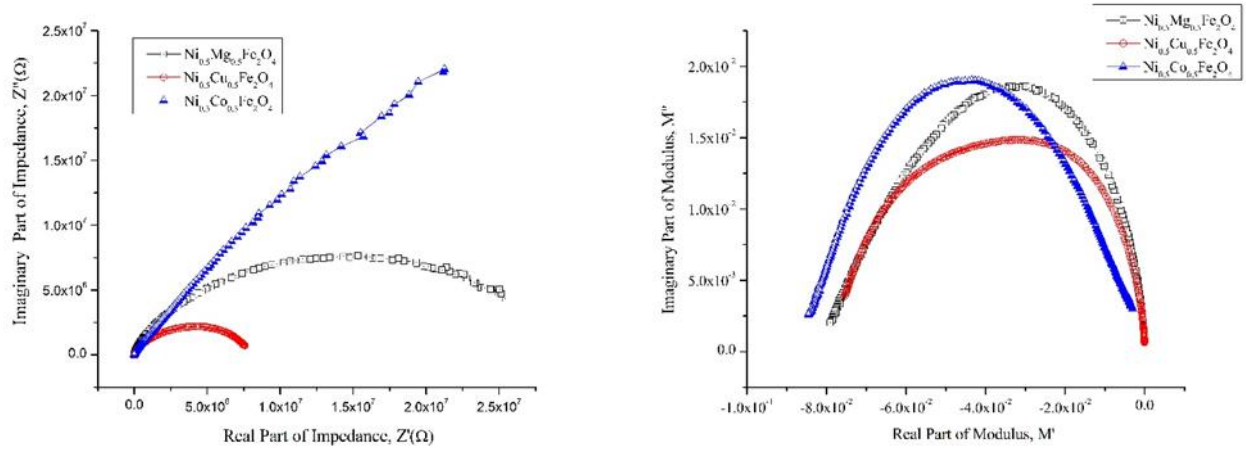

Fig. 3 Variation of Real and Imaginary Parts of Impedance and electric modulus (i) Z' Vs Z" and (j) M' Vs M".

Gas Sensing Studies

In this, the potentiality of the spinel structure ferrites doped with divalent metal ions is explored for gas sensing particularly for NO_2 gas (for 100ppm). Change of resistance usually mentioned as R_a/R_g, where Ra, the resistance in air, R_g, the resistance of the sensor after exposing to the gas, is the response which is the main performance of a gas sensor [21-22]. When doped ferrite samples based sensor is exposed to the air, the oxygen molecules in the air will chemisorb onto the metal oxide particle, capturing the electrons and transforms into O_2^-, O^- or O_2^-which specifically depends on temperature shown in equations (1) to (4). Mechanism of NO_2 detection of tested sensors (samples) at RT can be explained by the chemisorption and removal of the surface chemisorbed species.

$$O_2\ (gas) \leftrightarrow O_2\ (ads) \quad (1)$$

$$O_2\ (ads) + e^- \leftrightarrow O_2^-\ (ads)\ T< 147^\circ C \quad (2)$$

$$O_2^-\ (ads) + e^- \leftrightarrow 2\ O^-\ (ads)\ 147^\circ C< T< 397^\circ C \quad (3)$$

$$O^-\ (ads) + e^- \leftrightarrow O^{2-}\ (ads)\ T> 397^\circ C \quad (4)$$

$$Fe^{+3} + e^- \leftrightarrow Fe^{+2} \quad \text{(n-type material)} \quad (5)$$

$$Ni^{+2} + h^+ \leftrightarrow Ni^{+3} \quad \text{(p-type material)} \quad (6)$$

$$G\ (gas) \leftrightarrow G\ (ads) \quad (7)$$

$$G\ (ads) + O- \rightarrow GO + e- \quad 147^\circ C< T< 397^\circ C \quad (8)$$

$$NO_2 + e^- \rightarrow NO_2^-\ (ads) \quad (9)$$

Electron transfers that occur in equations (2) – (4) cause the formation of the depletion layer on the materials surface, making the conductive channel narrow with the the increase of R_a (Resistance in air). During the sensing process, the chemisorbed oxide particle can capture electrons, changing Fe^{+2} to Fe^{+3}, which is shown in equation (5). In p-type

material, the hole becomes the carrier as per equation (6). On account of the dissociation effect of oxygen, the valency distribution and defects in the crystal structure changed, while a part of the conductive three-dimensional network structure is cut off, so that the R_a of the material increases [21-22].

When the reduced gas diffuses to the surface of the sensitive material, it will rapidly undergo a redox reaction, with the oxygen on the surface. During the reaction, electron captured by oxygen will return to the material, and the resistance will be altered means decreases. According to the sensing mechanism, the possible reacting processes to reduced gas are as per the equations (7) and (8). Detailed reaction will change with the operating temperature. Similar explanation follows for the remaining series of composite samples. Sensing response of doped $NiFe_2O_4$, samples are mentioned from Fig. 4. Obtained sensing parameters for NO_2 gas sensing is tabulated in Table.1. From the obtained data, it is clear that among the doped samples $Ni_{0.5}Cu_{0.5}Fe_2O_4$-NCu-2 shown good sensing properties in when compared to remaining two samples in terms of response time and recovery time, it is because of the surface properties of the sample such as its particle size, porous structure of the sample, which can be further confirmed from optical microscopy studies (FESEM) [23-25].

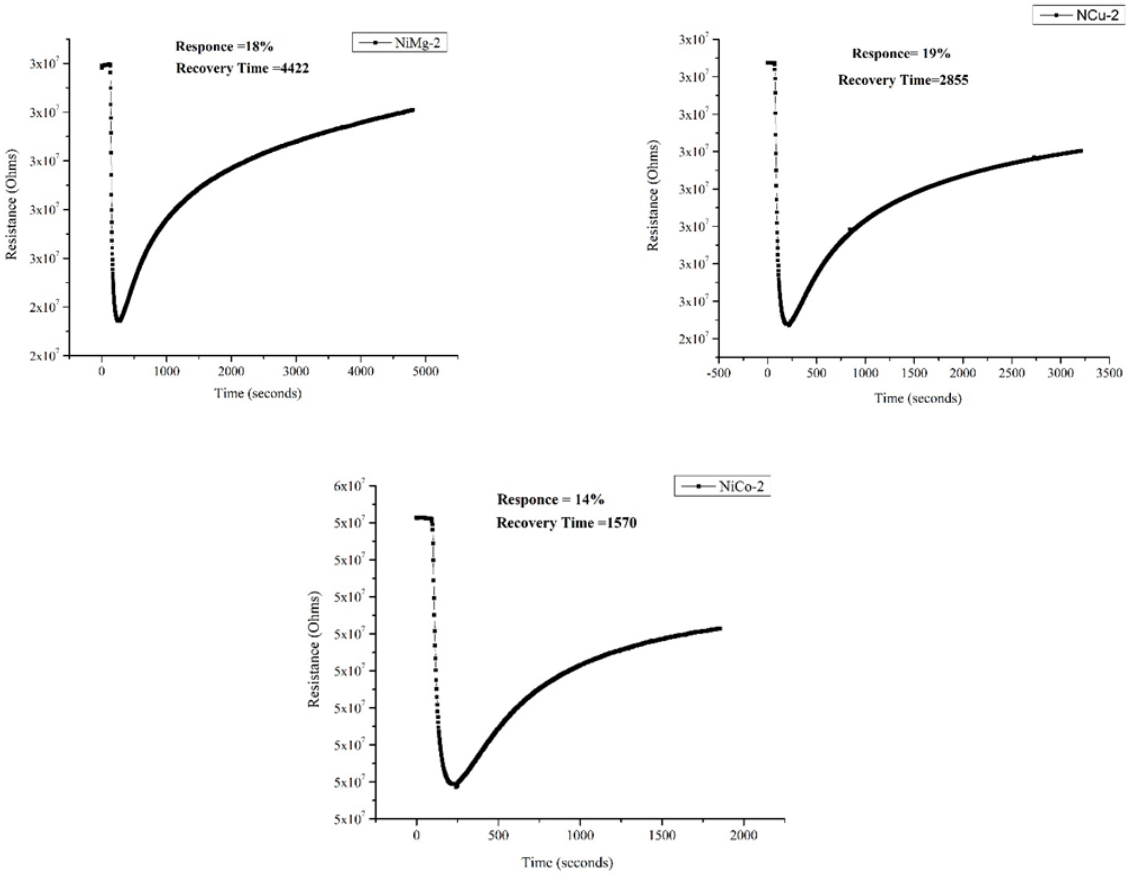

Fig. 4. NO_2 Gas sensing response of Ni (Mg, Cu, Co) Fe_2O_4 nano-powders.

Table 1. Gas sensing parameters obtained from sensing measurements.

Sample	Response of sensor in percentage	Recovery time in seconds
NiMg-2	18	4422
NCu-2	19	2855
NiCo-2	14	1570

Conclusions

Nano-powders of the system $Ni_{0.5}M_{0.5}Fe_2O_4$ (here M=Mg^{+2}, Cu^{+2}, Co^{+2}) were prepared successfully using auto-combustion method which involves nitrate-citrate precursors. Structural phase is confirmed through PXRD studies for the divalent metal ions doped $NiFe_2O_4$ nano samples. Morphology of the nano-powders reveals the dense structures with well-defined grains. All the proposed samples responded to NO_2 gas, enabling them suitable candidates for NO_2 detection or sensing.

Finally, it is concluded that, series of divalent metal ions doped ferrite samples have been studied for impedance and gas sensing properties. These characteristics of the proposed nano-powder samples are of technologically important and can be implemented in smart functional device applications.

Acknowledgements

Authors are highly thankful to CENSE, IISc-Bangalore for providing PXRD and FESEM facilities to accomplish this research work.

References

1. G. Y Zhang, C. S Li, F. Y Cheng, Sens. Actuators B, 246, PP.662-672 (2007)
2. X.S Niu, W.P Du, W.M Du, Sens. Actuators B, 99, pp.405-409.
3. C. Mukherjee , R. Mondal, S. Dey, S. Kumar. IEEE Sens. Jour ,17, pp.2662-2669 (2004).
4. Valenzuela R, Phys. Res.Int, 2012 (2012).
5. J Liu, S Li, B. Zhang, Y. L Wang, Y.Gao, X.S Liang, Y.Wang, J.Colloid Intface.Sci,504, pp.206-213 (2017).
6. T. V A Kusuman, V. S Siril, K. N Madhusoodanan, N. K Renuka, Sen. Actuators A 318, pp.112389 (2021).
7. I.Kortidis, H.C Swart, S.S Ray, D.E Motaung, Sen.Actu B Chem, 285, pp.92-107 (2019).
8. M.Lakshmi, K.Vijaya kr, K.Thyagarajan , J.Nano.struct in Chem, 5(4), pp.365 (2015).
9. Abdallah H M I, Moyo T, Ngema N, Jour.Magn.Magn. Matr, 394, pp.223-228 (2015).
10.A.B Bodade, H.G Wankhade, G.N Chaudhari, D.C Kothari, Talanta, 89, pp.183 (2012).
11.S.Abdul Khader, Asiya Parveez, Arka Chaudhuri, M S Shekhawat and T.Sankarappa, Physica B: Condensed Matter, 584, May Issue, pp.411675 (2020).
12.K. Mukherjee, S.B Majumder, Jour. Talanta, 81, pp.1826-1832 (2010).
13.S.Andris, G.A Karlis, Sens. Actuators B, 222, pp.95-105 (2016).
14.Wagner KW (1913) Ann Phys 40:817.
15.Maxwell JC, Electricity & Magnetism, Vol 1, Oxford Univ Press, Oxford (1929).
16.Koops CG (1951) Phys Rev 83:121.
17.J.Smitet H.P, J Wijn, Les.Ferrites, Dunod, Paris (1961).
18.P.Singh, D.Rathore, Jour. Appl. Phys, 1728, pp.20259 (2016).
19.Chikazumi S, Physics of Ferromagnetism, Oxford University Press, Oxford (1997).
20.E.C Stoner and E.P Wohlfarth. Phil. Trans. Roy. Soc.A 240, 599 (1948).
21.P. Shankar and J.B. B Rayappan, Sci.Lett. J, 4, pp.126 (2015).
22.G. Erannna, Solid state Gas Sensing, Springer Publications (2009).
23.D.Rathore, R.Kurchania, R.K Pandey, J.Nano Sci. Nanotech, 13, pp.1812-1819 (2013).
24. S.Sen, P.Anand, M.Narjinary, S.K Md Mursalin, R.Manna, Ceramic Int, 42,pp.12581 (2016).
25.S.Peng, M.Ma, W.Yang, Z.Wang, J.Bi, Sens.Actuators B, 190, pp.627-633 (2014).